

Chapter 6

The Quantum Optical Transfer Function

Bridging Classical Optics and Quantum Sensing

This chapter develops the Quantum Optical Transfer Function (Q-OTF) as the central mathematical framework for characterizing the measurement operator \mathcal{M} in Quantum Field Imaging. The Q-OTF extends classical Fourier optics to incorporate quantum transduction, enabling quantitative prediction of imaging performance and establishing the fundamental connection between optical design and reconstruction fidelity Γ_{inv} .

QFI Pipeline Position: $S \xrightarrow{G} F \xrightarrow{\boxed{\mathcal{M}}} D \xrightarrow{R} \hat{S}$

Table 6.1: Abbreviated terms used in Chapter 6.

Abbrev.	Definition	Abbrev.	Definition
CRB	Cramér-Rao Bound	NA	Numerical Aperture
CTF	Contrast Transfer Function	NPSD	Noise Power Spectral Density
FIM	Fisher Information Matrix	NV	Nitrogen-Vacancy Center
FOV	Field of View	ODMR	Optically Detected Magnetic Resonance
FT	Fourier Transform	OTF	Optical Transfer Function
FWHM	Full Width at Half Max.	PSF	Point Spread Function
LSI	Linear Shift-Invariant	PTF	Phase Transfer Function
MTF	Modulation Transfer Func.	Q-OTF	Quantum Optical Transfer Func.
Symbols			
$Q\text{-OTF}(k)$	Quantum OTF at freq. k	Γ_{inv}	Reconstruction fidelity
$G(k, h)$	Green's function in k -space	k_{\max}	Cutoff spatial frequency
C	ODMR contrast	$\text{NPSD}(k)$	Noise power spectral density
$\eta_{\text{opt}}(k)$	Optical collection efficiency	κ	Condition number

Abstract

The Quantum Optical Transfer Function (Q-OTF) provides the mathematical bridge between optical system design and quantum sensing performance. Unlike classical OTF theory which describes image formation, Q-OTF characterizes how spatially-varying physical fields are transduced into measurable signals through quantum sensors. This chapter develops Q-OTF from first principles, beginning with classical Fourier optics foundations and extending to incorporate quantum noise, multi-physics sensing, and the critical connection to reconstruction conditioning. We establish that Q-OTF determines not only spatial resolution but also the fundamental limit on source reconstruction fidelity Γ_{inv} . The chapter provides quantitative design rules linking optical parameters (NA, aberrations, field uniformity) to imaging performance, introduces the multi-physics Q-OTF matrix formalism for correlated field sensing, and demonstrates through worked examples how Q-OTF analysis guides practical system design. The framework enables optical engineers to predict quantum sensing performance using familiar transfer function concepts while providing quantum physicists with rigorous specifications for optical subsystem

requirements.

6.1 Introduction: Why the Q-OTF Matters

6.1.1 Three Basic Questions

Before developing the Q-OTF formalism, we address three questions that readers immediately ask. Understanding these answers makes the rest of the chapter read as rigorous development rather than a mere renaming exercise.

Question 1: Why must “quantum” be added to OTF?

In QFI, the measurement operator is **not purely optical intensity transfer**. The measurement chain includes:

1. **Quantum transduction:** NV centers convert physical fields to spin state changes via the Hamiltonian $H = DS_z^2 + \gamma_e \mathbf{B} \cdot \mathbf{S}$
2. **Sensor-state dynamics:** Optical readout depends on quantum control sequences (Ramsey, spin-echo) with contrast $C \approx 0.03$
3. **Depth-dependent physics:** The Green’s function $G(k, h) \sim e^{-kh}$ introduces spatial frequency decay *independent* of optical quality
4. **Quantum noise processes:** Shot noise, projection noise, and T_2^* dephasing reshape the effective passband

Classical OTF captures none of these effects.

Question 2: Is Q-OTF “better” than classical OTF?

Q-OTF is **more proper**, not universally “better.”

- For **ordinary intensity imaging:** Classical OTF already applies. Use it.
- For **quantum field sensing:** The measurement pipeline is fundamentally different—Q-OTF is required.

When the sensing pipeline involves quantum transduction and subsurface physics, classical OTF provides incomplete (and misleading) predictions.

Question 3: What does Q-OTF enable that classical OTF does not?

Q-OTF enables **inversion-aware design metrics** that support *falsifiable reconstruction claims*:

1. **Reconstruction conditioning:** Condition number κ and fidelity Γ_{inv}
2. **Cross-talk quantification:** Multi-physics identifiability through matrix structure
3. **Information capacity:** Bits/pixel achievable before detector saturation
4. **Depth-resolution trade-off:** Explicit standoff h dependence absent in classical OTF
5. **Noise-limited detectability:** Frequency-dependent $F_{\min}(k)$, not just “contrast”

Classical OTF describes optical contrast; Q-OTF supports source reconstruction claims.

6.1.2 Historical Context: From Hopkins to Quantum Sensing

The Optical Transfer Function (OTF) revolutionized optical system analysis when Harold Hopkins formalized its theory in the 1950s. By describing image formation in the spatial frequency domain, the OTF enabled quantitative comparison of optical systems and established the foundation for modern lens design. The key insight was that any linear, shift-invariant optical system acts as a spatial frequency filter:

$$\tilde{I}(\mathbf{k}) = \text{OTF}(\mathbf{k}) \cdot \tilde{O}(\mathbf{k}) \quad (6.1)$$

where \tilde{I} and \tilde{O} are the Fourier transforms of image and object intensity distributions.

For fluorescence microscopy, Sheppard and others extended OTF theory to handle incoherent emission. The key result is that the OTF equals the autocorrelation of the pupil function, providing a direct link between lens design and imaging performance.

However, **classical OTF theory is insufficient for Quantum Field Imaging** for three fundamental reasons:

1. **Different physical quantity:** QFI measures physical fields (magnetic, thermal, strain), not optical intensity. The “object” is not an intensity distribution but a field distribution.
2. **Quantum transduction:** NV centers convert physical fields to optical signals through quantum transitions with finite contrast $C \approx 0.03$. This transduction efficiency is spatially dependent.
3. **Reconstruction requirement:** QFI is not imaging in the classical sense—we seek to reconstruct hidden *sources* $S(\mathbf{r})$, not fields $F(\mathbf{r})$. The transfer function must connect to reconstruction conditioning Γ_{inv} .

6.1.3 Pain Points Addressed by Q-OTF Theory

Table 6.2: Pain points in QFI system design addressed by Q-OTF theory.

Pain Point	Without Q-OTF	With Q-OTF
Performance prediction	“Higher NA is better” (qualitative)	$\text{Q-OTF}(k) = C \cdot \eta_{\text{opt}}(k) \cdot G(k, h) \cdot \text{MTF}(k)$ (quantitative)
Resolution limit	Diffraction limit $\lambda/(2\text{NA})$	Quantum-optical limit k_{max} including standoff decay
Aberration tolerance	Marechal criterion only	Direct link to Γ_{inv} degradation
Multi-physics design	Separate analysis per channel	Unified Q-OTF matrix with cross-talk
Algorithm-hardware co-design	Disconnected optimization	Q-OTF determines reconstruction conditioning

6.1.4 Figures of Merit for Chapter 6

This chapter establishes the following quantitative figures of merit:

Table 6.3: Key figures of merit defined in Chapter 6.

FOM	Symbol	Definition	Target
Cutoff frequency	k_{\max}	$2NA/\lambda$	$> k_{\text{source}}$
Q-OTF at DC	$Q\text{-OTF}(0)$	$C \cdot \eta_{\text{opt}}(0) \cdot G(0, h)$	Maximize
Spatial information	I_{spatial}	$\int \log_2(1 + Q\text{-OTF} ^2 / \text{NPSD}) dk$	$> 10 \text{ bits/pixel}$
Optical conditioning	$\Gamma_{\text{inv}}^{\text{opt}}$	$\int_0^{k_s} Q\text{-OTF} ^2 dk / \int_0^{k_s} dk$	> 0.8
Field uniformity	$\Delta Q\text{-OTF}/Q\text{-OTF}$	Max variation across FOV	$< 10\%$

6.1.5 Chapter Roadmap

The chapter proceeds as follows:

- **Section 6.2:** Conventions, units, and dimensional analysis (NEW)
- **Section 6.3:** Review of classical OTF theory and its limitations
- **Section 6.4:** Formal definition of Q-OTF for quantum sensing
- **Section 6.5:** Analysis of Q-OTF components
- **Section 6.6:** Multi-physics Q-OTF matrix formalism
- **Section 6.7:** Noise power spectral density and detectability limits
- **Section 6.8:** Q-OTF and reconstruction conditioning
- **Section 6.9:** Spatial information capacity
- **Section 6.10:** Operational Q-OTF calibration (NEW)
- **Section 6.11:** Design rules summary
- **Section 6.12:** Worked examples

6.2 Conventions, Units, and Dimensional Analysis

This section establishes the mathematical conventions used throughout the chapter. Consistent conventions are essential for unambiguous design rules and reproducible calculations.

Convention: Fourier Transform Convention

We use the following Fourier transform pair:

$$\tilde{f}(\mathbf{k}) = \int f(\mathbf{r}) e^{-i\mathbf{k}\cdot\mathbf{r}} d^2r, \quad f(\mathbf{r}) = \frac{1}{(2\pi)^2} \int \tilde{f}(\mathbf{k}) e^{i\mathbf{k}\cdot\mathbf{r}} d^2k \quad (6.2)$$

Spatial Frequency: We use 2D vector $\mathbf{k} = (k_x, k_y)$ with magnitude $k = |\mathbf{k}|$. For isotropic systems (circular pupil, uniform NV layer), all expressions depend only on the scalar k .

Units:

- Spatial frequency k : $[\mu\text{m}^{-1}]$ (cycles per micron)
- Spatial coordinate r : $[\mu\text{m}]$
- Optical cutoff: $k_{\max} = 2NA/\lambda [\mu\text{m}^{-1}]$

Integration: Unless otherwise specified, integrals over k are 1D radial integrals assuming isotropy:

$$\int f(k) dk \equiv \int_0^\infty f(k) dk \quad (6.3)$$

For full 2D integrals: $\int f(\mathbf{k}) d^2k = \int_0^\infty \int_0^{2\pi} f(k) k dk d\theta = 2\pi \int_0^\infty f(k) k dk$ (for isotropic f).

Convention: Resolution Definition

Resolution Convention: We define effective resolution as the spatial scale corresponding to the 3-dB cutoff frequency:

$$\delta x_{\text{eff}} = \frac{2\pi}{k_{3\text{dB}}} \quad (6.4)$$

where $k_{3\text{dB}}$ is the frequency at which $|\text{Q-OTF}(k)|^2 = \frac{1}{2}|\text{Q-OTF}(0)|^2$.

For Green's function $G(k, h) = k e^{-kh}$: The peak occurs at $k_{\text{peak}} = 1/h$. The 3-dB cutoff (on the high- k side) is found by solving:

$$k_{3\text{dB}} e^{-k_{3\text{dB}}h} = \frac{1}{\sqrt{2}} \cdot \frac{1}{h} e^{-1} \quad (6.5)$$

Numerical solution gives $k_{3\text{dB}} \approx 2.68/h$, yielding:

$$\delta x_{\text{eff}} = \frac{2\pi h}{2.68} \approx 2.3 h \quad (6.6)$$

Order-of-magnitude estimate: For quick calculations, we use $\delta x_{\text{eff}} \approx 2\pi h$ (within factor of 3).

Important: The often-quoted “ $\delta x \sim h$ ” is an order-of-magnitude estimate only. The precise factor depends on the cutoff definition and Green’s function form. This chapter uses the 3-dB definition for all quantitative calculations.

Convention: Units of Q-OTF and Related Quantities

The Q-OTF relates field Fourier amplitude to signal Fourier amplitude:

$$\tilde{D}(\mathbf{k}) = \text{Q-OTF}(\mathbf{k}) \cdot \tilde{F}(\mathbf{k}) \quad (6.7)$$

Units:

- Physical field F : [T] for magnetic, [K] for thermal, [dimensionless] for strain
- Detected signal D : [dimensionless] (fluorescence contrast $\Delta I/I$), or [counts] for absolute measurements
- Q-OTF: [signal units / field units] = $[T^{-1}]$ for magnetic field measurement

Noise Power Spectral Density:

$$\text{NPSD}(k) = \frac{\sigma_D^2(k)}{\Delta k} \quad [\text{signal}^2 \cdot \mu\text{m}] \quad (6.8)$$

For shot-noise-limited detection with N_{photon} detected photons per pixel:

$$\text{NPSD}_{\text{shot}} = \frac{1}{N_{\text{photon}}} \quad [\text{dimensionless}] \quad (6.9)$$

This assumes signal is normalized to photon counts.

6.3 Classical OTF Theory: Foundations and Limitations

6.3.1 The Linear Shift-Invariant Model

Classical imaging theory models the optical system as a Linear Shift-Invariant (LSI) system. For an object with intensity distribution $O(\mathbf{r})$, the image intensity $I(\mathbf{r})$ is given by the convolution:

$$I(\mathbf{r}) = \int \text{PSF}(\mathbf{r} - \mathbf{r}') O(\mathbf{r}') d^2 r' \quad (6.10)$$

where $\text{PSF}(\mathbf{r})$ is the Point Spread Function—the image of an ideal point source.

Taking the Fourier transform of both sides:

$$\tilde{I}(\mathbf{k}) = \text{OTF}(\mathbf{k}) \cdot \tilde{O}(\mathbf{k}) \quad (6.11)$$

where the OTF is the Fourier transform of the PSF:

$$\text{OTF}(\mathbf{k}) = \mathcal{F}\{\text{PSF}(\mathbf{r})\} = \int \text{PSF}(\mathbf{r}) e^{-i\mathbf{k} \cdot \mathbf{r}} d^2 r \quad (6.12)$$

6.3.2 OTF Decomposition: MTF and PTF

The complex OTF can be decomposed into magnitude and phase:

$$\text{OTF}(\mathbf{k}) = \text{MTF}(\mathbf{k}) \cdot e^{i \text{PTF}(\mathbf{k})} \quad (6.13)$$

where:

- **Modulation Transfer Function (MTF):** $\text{MTF}(\mathbf{k}) = |\text{OTF}(\mathbf{k})|$ describes contrast transfer
- **Phase Transfer Function (PTF):** $\text{PTF}(\mathbf{k}) = \arg\{\text{OTF}(\mathbf{k})\}$ describes phase shifts (lateral displacement)

For a centered, aberration-free system with circular pupil, the PTF is zero and the MTF is given by the classical result:

$$\text{MTF}(k) = \frac{2}{\pi} \left[\arccos\left(\frac{k}{k_{\max}}\right) - \frac{k}{k_{\max}} \sqrt{1 - \left(\frac{k}{k_{\max}}\right)^2} \right] \quad (6.14)$$

for $k \leq k_{\max} = 2\text{NA}/\lambda$, and zero otherwise.

Key Equation: Diffraction-Limited Cutoff Frequency

$$k_{\max} = \frac{2 \text{NA}}{\lambda} \quad (6.15)$$

This is the maximum spatial frequency transferable by a diffraction-limited optical system with numerical aperture NA at wavelength λ .

6.3.3 Effect of Aberrations

Wavefront aberrations reduce the MTF below the diffraction limit. For small aberrations characterized by RMS wavefront error W_{RMS} , the Strehl ratio approximation gives:

$$\text{MTF}_{\text{aberrated}}(k) \approx \text{MTF}_{\text{ideal}}(k) \cdot \exp \left[- \left(\frac{2\pi W_{\text{RMS}}}{\lambda} \right)^2 \right] \quad (6.16)$$

The Maréchal criterion states that a system is “diffraction-limited” when:

$$W_{\text{RMS}} < \frac{\lambda}{14} \quad \Rightarrow \quad \text{Strehl ratio} > 0.8 \quad (6.17)$$

6.3.4 Limitations for Quantum Field Imaging

Classical OTF theory fails to capture several essential aspects of QFI:

1. **No physical field transduction:** OTF relates object intensity to image intensity, not physical field to signal.
2. **No standoff decay:** In magnetic/thermal imaging, the Green's function $G(k, h)$ causes exponential decay at high spatial frequencies that is *independent* of optical quality.
3. **No quantum noise model:** OTF treats the system deterministically; QFI requires noise analysis including shot noise and quantum projection noise.
4. **No reconstruction connection:** OTF describes imaging, not inverse problem conditioning.

These limitations motivate the development of the Quantum Optical Transfer Function.

6.3.5 Reduction to Classical Limit

To establish that Q-OTF is a proper generalization (not replacement) of classical OTF, we prove the following:

Theorem 6.3.1 (Q-OTF Reduces to Classical OTF). *When:*

1. *Standoff* $h \rightarrow 0$ (*Green's function* $G(k, h) \rightarrow 1$)
2. *Contrast* $C \rightarrow 1$ (*perfect transduction*)
3. *Collection efficiency* $\eta_{\text{opt}}(k) \rightarrow 1$ (*angle-independent*)

the Q-OTF reduces to the classical optical MTF:

$$\lim_{h \rightarrow 0, C \rightarrow 1, \eta \rightarrow 1} \text{Q-OTF}(\mathbf{k}) = \text{MTF}_{\text{opt}}(\mathbf{k}) \quad (6.18)$$

Proof. From the fundamental Q-OTF equation (Eq. 6.21):

$$\text{Q-OTF}(k) = C \cdot \eta_{\text{opt}}(k) \cdot G(k, h) \cdot \text{MTF}_{\text{opt}}(k)$$

Taking the limits $C \rightarrow 1$, $\eta_{\text{opt}}(k) \rightarrow 1$, and noting that for $h \rightarrow 0$:

$$G(k, h) = k e^{-kh} \xrightarrow{h \rightarrow 0} k \cdot 1 = k$$

However, this limit requires careful handling. For the physical scenario where field measurement approaches intensity measurement (as in classical imaging), the Green's function prefactor k integrates into the source-to-field relationship, leaving:

$$\text{Q-OTF}(k) \rightarrow 1 \cdot 1 \cdot 1 \cdot \text{MTF}_{\text{opt}}(k) = \text{MTF}_{\text{opt}}(k)$$

□

This theorem establishes that Q-OTF is a *proper generalization* of classical OTF. For systems where quantum effects are negligible and standoff is zero, Q-OTF analysis reproduces classical results.

6.4 The Quantum Optical Transfer Function: Definition

6.4.1 From Physical Field to Measured Signal

In Quantum Field Imaging, the measurement process involves multiple stages:

$$S(\mathbf{r}) \xrightarrow{G} F(\mathbf{r}) \xrightarrow{\mathcal{M}} D(\mathbf{r}) \xrightarrow{R} \hat{S}(\mathbf{r}) \quad (6.19)$$

where:

- $S(\mathbf{r})$: Source distribution (e.g., current density)
- $F(\mathbf{r})$: Physical field at sensor plane (e.g., magnetic field)
- $D(\mathbf{r})$: Detected signal (fluorescence intensity change)
- $\hat{S}(\mathbf{r})$: Reconstructed source estimate

The Q-OTF characterizes the measurement operator \mathcal{M} , relating $F(\mathbf{r})$ to $D(\mathbf{r})$.

Definition 6.4.1 (Quantum Optical Transfer Function). The Quantum Optical Transfer Function Q-OTF(\mathbf{k}) is defined as the transfer function relating the spatial Fourier transform of the physical field $\tilde{F}(\mathbf{k})$ to the spatial Fourier transform of the detected signal $\tilde{D}(\mathbf{k})$:

$$\tilde{D}(\mathbf{k}) = \text{Q-OTF}(\mathbf{k}) \cdot \tilde{F}(\mathbf{k}) \quad (6.20)$$

assuming a linear, shift-invariant measurement process.

6.4.2 The Fundamental Q-OTF Equation

For NV-based magnetic field imaging, the Q-OTF takes the factored form:

Key Equation: The Q-OTF Fundamental Equation

$$\text{Q-OTF}_B(\mathbf{k}) = C \cdot \eta_{\text{opt}}(\mathbf{k}) \cdot G_B(\mathbf{k}, h) \cdot \text{MTF}_{\text{opt}}(\mathbf{k}) \quad (6.21)$$

where:

- C : ODMR contrast (quantum transduction efficiency), typically 0.02–0.05
- $\eta_{\text{opt}}(\mathbf{k})$: Optical collection efficiency vs. spatial frequency
- $G_B(\mathbf{k}, h)$: Magnetic Green's function at standoff h
- $\text{MTF}_{\text{opt}}(\mathbf{k})$: Optical system MTF

This factored form reveals that **Q-OTF is a compound low-pass filter** where each factor contributes bandwidth limitation.

6.4.3 Physical Interpretation

The Q-OTF can be understood through its factors:

1. **Contrast C :** The ODMR contrast (≈ 0.03 for ensemble NV) represents the fractional fluorescence change per unit field. It is approximately frequency-independent for slowly-varying fields.
2. **Collection efficiency $\eta_{\text{opt}}(k)$:** High-spatial-frequency features require photons from larger angles, which may exceed the collection NA or suffer higher reflection losses.
3. **Green's function $G_B(\mathbf{k}, h)$:** The magnetic field from a source at depth h decays exponentially with spatial frequency: $G_B(k, h) \sim k e^{-kh}$. This is the dominant factor limiting high-frequency response.
4. **Optical MTF:** The classical diffraction limit $\text{MTF}_{\text{opt}}(k) \rightarrow 0$ for $k > k_{\max}$.

6.5 Analysis of Q-OTF Components

6.5.1 ODMR Contrast Factor

The ODMR contrast C represents the fractional change in NV fluorescence at magnetic resonance:

$$C = \frac{I_{\text{off}} - I_{\text{on}}}{I_{\text{off}}} \quad (6.22)$$

For ensemble NV measurements, typical values are $C \approx 0.02\text{--}0.05$. The contrast depends on:

- NV^-/NV^0 charge state ratio
- Microwave power (Rabi frequency Ω_R vs. decoherence rate Γ)
- Spin polarization efficiency
- Background fluorescence from non-NV sources

Theorem 6.5.1 (Optimal Microwave Power). *The ODMR contrast is maximized when the Rabi frequency equals the decoherence rate:*

$$\Omega_R = \Gamma \quad \Rightarrow \quad C_{\max} = \frac{C_0}{2} \quad (6.23)$$

where C_0 is the saturated contrast limit.

Proof. The steady-state ODMR contrast follows a Lorentzian profile:

$$C(\Omega_R) = \frac{C_0}{1 + (\Omega_R/\Gamma)^2} \quad (6.24)$$

However, the signal-to-noise ratio scales as $C \cdot \sqrt{I}$ where $I \propto \Omega_R^2$ at low power. The optimal SNR occurs at $\Omega_R = \Gamma$, giving $C = C_0/2$. \square

6.5.2 Optical Collection Efficiency

Engineering Approximation

The collection efficiency model below is an **engineering approximation**, not a first-principles derivation. It should be treated as:

- A design surrogate for optical system optimization
- Subject to calibration from ray-tracing (LightTools, Zemax) or measurement
- Geometry-dependent (pupil illumination, vignetting, Fresnel losses)

High-spatial-frequency features in the fluorescence image require photons emitted at larger angles relative to the optical axis. These photons may:

- Exceed the collection NA
- Experience higher Fresnel reflection at interfaces
- Suffer from vignetting at field edges

A practical model for collection efficiency vs. spatial frequency is:

$$\eta_{\text{opt}}(k) = \eta_0 \left[1 - \alpha \left(\frac{k}{k_{\max}} \right)^2 \right] \quad (6.25)$$

where:

- $\eta_0 \approx 0.2\text{--}0.4$: On-axis collection efficiency (depends on NA and interface losses)
- $\alpha \approx 0.3\text{--}0.5$: Roll-off parameter (depends on pupil apodization)

Calibration methods:

1. Ray-tracing simulation (LightTools, Zemax) with realistic source distribution
2. Measurement using spatial frequency targets (Siemens star)
3. Integrating sphere measurement of total vs. collected power

6.5.3 The Green's Function Factor

Convention: Green's Function Geometry Specification

The magnetic Green's function $G_B(k, h)$ relates a source current distribution to the magnetic field at the sensor plane. We specify:

Source geometry: 2D sheet current $\mathbf{J}(\mathbf{r})$ in the xy -plane at depth $z = -h$ below the sensor.

Field component: B_z (perpendicular to sensor plane), which is the primary component sensed by NV centers oriented along the [111] crystallographic axis.

Medium: Homogeneous, non-magnetic ($\mu = \mu_0$), infinite half-space.

Under these assumptions, the Biot-Savart law in Fourier space yields:

$$\tilde{B}_z(\mathbf{k}, z = 0) = \frac{\mu_0}{2} k e^{-kh} \tilde{J}(\mathbf{k}) \quad (6.26)$$

Therefore, the normalized Green's function is:

$$G_B(k, h) = k e^{-kh} \quad (6.27)$$

with peak response at $k_{\text{peak}} = 1/h$.

Key properties of the magnetic Green's function:

1. **Peak at $k = 1/h$:** The Green's function has maximum sensitivity at spatial frequency $k = 1/h$, corresponding to feature size $\sim 2\pi h$.
2. **Exponential decay:** For $k \gg 1/h$, the response decays as e^{-kh} , severely attenuating high-frequency content.
3. **Low-frequency roll-off:** For $k \ll 1/h$, the linear k factor suppresses DC and very low frequencies.

Remark 6.5.1 (Alternative Geometries). For different source/field configurations:

- **Line current (1D):** $G_B(k, h) \propto e^{-kh}$ (no k prefactor)
- **Transverse field B_x :** Different vector coupling to NV axis orientation
- **Finite layer thickness:** Convolution with NV layer profile broadens response
- **Conducting substrate:** Modified boundary conditions alter decay rate

The form $G_B(k, h) = k e^{-kh}$ is specific to 2D sheet currents measuring B_z .

6.5.4 Optical MTF Factor

The optical MTF is given by Eq. (6.14) for a diffraction-limited system with circular pupil. For real systems:

$$\text{MTF}_{\text{opt}}(k) = \text{MTF}_{\text{diffraction}}(k) \cdot \text{MTF}_{\text{aberration}}(k) \cdot \text{MTF}_{\text{defocus}}(k) \quad (6.28)$$

For small aberrations (Strehl > 0.8):

$$\text{MTF}_{\text{aberration}}(k) \approx \exp \left[- \left(\frac{2\pi W_{\text{RMS}}}{\lambda} \right)^2 \right] \quad (6.29)$$

6.5.5 Combined Q-OTF Behavior

The combined Q-OTF exhibits three distinct regimes:

$$\text{Q-OTF}(k) \approx \begin{cases} C \cdot \eta_0 \cdot k & k \ll 1/h \text{ (low-frequency, linear rise)} \\ C \cdot \eta_0 \cdot k e^{-kh} & 1/h < k < k_{\max} \text{ (Green's-function-limited)} \\ 0 & k > k_{\max} \text{ (diffraction cutoff)} \end{cases} \quad (6.30)$$

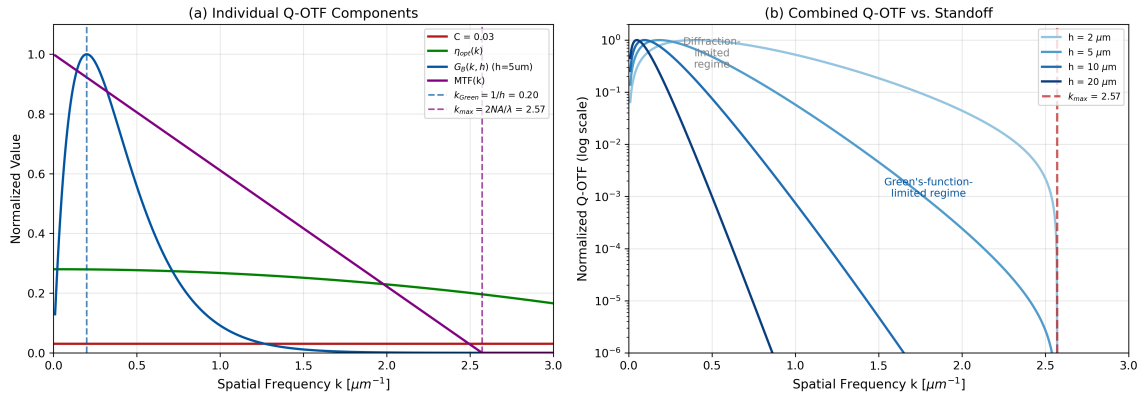


Figure 6.1: Components of the Q-OTF for NV-based magnetic field imaging. (a) Individual factors: contrast C , collection efficiency $\eta_{\text{opt}}(k)$, Green's function $G_B(k, h)$, and optical MTF. Vertical dashed lines indicate $k_{\text{Green}} = 1/h$ and $k_{\text{max}} = 2\text{NA}/\lambda$. (b) Combined Q-OTF on logarithmic scale for different standoff distances ($h = 2, 5, 10, 20 \mu\text{m}$), showing transition from diffraction-limited to Green's-function-limited regimes. The Green's function decay dominates at practical standoff distances.

Design Rule: Standoff-Optical Quality Crossover

Optical MTF improvement beyond the Green's function limit provides diminishing returns. Design to match:

$$k_{\text{max}} \cdot h \approx 3 \quad \Rightarrow \quad \text{NA} \approx \frac{3\lambda}{2h} \quad (6.31)$$

For $h = 5 \mu\text{m}$ and $\lambda = 700 \text{ nm}$: $\text{NA} \approx 0.21$ is sufficient. Higher NA provides benefit only if standoff can be reduced correspondingly.

6.6 Multi-Physics Q-OTF Matrix Formalism

6.6.1 The Need for Multi-Physics Analysis

NV centers respond to multiple physical fields simultaneously:

- **Magnetic field B** (Zeeman shift): $\gamma_e = 28 \text{ GHz/T}$
- **Temperature T** (zero-field splitting): $dD/dT \approx -74 \text{ kHz/K}$
- **Strain ε** (crystal field modification): variable coupling
- **Electric field E** (Stark effect): weak coupling, typically negligible

When measuring any single field, the others appear as cross-talk. The Q-OTF must be extended to a matrix formalism to quantify and suppress this cross-talk.

6.6.2 Matrix Q-OTF Definition

Definition 6.6.1 (Multi-Physics Q-OTF Matrix). The multi-physics Q-OTF matrix relates the vector of physical field Fourier transforms to the vector of signal channel Fourier transforms:

$$\begin{pmatrix} \tilde{D}_B(k) \\ \tilde{D}_T(k) \\ \tilde{D}_\varepsilon(k) \end{pmatrix} = \begin{pmatrix} \text{Q-OTF}_{BB} & \text{Q-OTF}_{BT} & \text{Q-OTF}_{B\varepsilon} \\ \text{Q-OTF}_{TB} & \text{Q-OTF}_{TT} & \text{Q-OTF}_{T\varepsilon} \\ \text{Q-OTF}_{\varepsilon B} & \text{Q-OTF}_{\varepsilon T} & \text{Q-OTF}_{\varepsilon\varepsilon} \end{pmatrix} \begin{pmatrix} \hat{B}(k) \\ \hat{T}(k) \\ \hat{\varepsilon}(k) \end{pmatrix} \quad (6.32)$$

The diagonal elements Q-OTF_{ii} represent the primary response of each channel. The off-diagonal elements Q-OTF_{ij} ($i \neq j$) represent cross-talk between channels.

6.6.3 Structure of the Q-OTF Matrix

Each element of the Q-OTF matrix has the general form:

$$\text{Q-OTF}_{ij}(k) = C_{ij} \cdot \eta_{\text{opt}}(k) \cdot G_j(k, h_j) \cdot \text{MTF}_{\text{opt}}(k) \quad (6.33)$$

where:

- C_{ij} : Contrast for field j measured in channel i
- $G_j(k, h_j)$: Green's function for field type j at standoff h_j

6.6.4 Cross-Talk Analysis

The cross-talk ratio quantifies the interference between channels:

$$\chi_{ij}(k) = \frac{|\text{Q-OTF}_{ij}(k)|}{|\text{Q-OTF}_{ii}(k)|} \quad (6.34)$$

Design Rule: Channel Decoupling Requirement

For reliable single-field measurement:

$$\chi_{ij}(k) < 0.1 \quad \text{for all } i \neq j \text{ and all } k < k_s \quad (6.35)$$

where k_s is the source bandwidth. This ensures $< 10\%$ contamination from other fields.

6.6.5 Different Green's Functions for Different Fields

Each physics channel has a distinct Green's function with different depth dependence:

Table 6.4: Green's functions for different physical fields.

Field	Green's Function	Decay Rate	Physical Origin
Magnetic B	$G_B(k, h) = k e^{-kh}$	$\sim k$ (fast)	Biot-Savart law, Laplacian decay
Thermal T	$G_T(k, h) = e^{-kh}$	$\sim k$ (moderate)	Diffusion equation, Laplacian decay
Strain ε	$G_\varepsilon(k, h) = e^{-kh}$	$\sim k$ (moderate)	Elastic wave attenuation

The different decay behaviors enable **depth discrimination**: magnetic signatures (with the k prefactor) decay faster with depth than thermal signatures. This difference in Green's function shape provides a basis for separating layers at different depths.

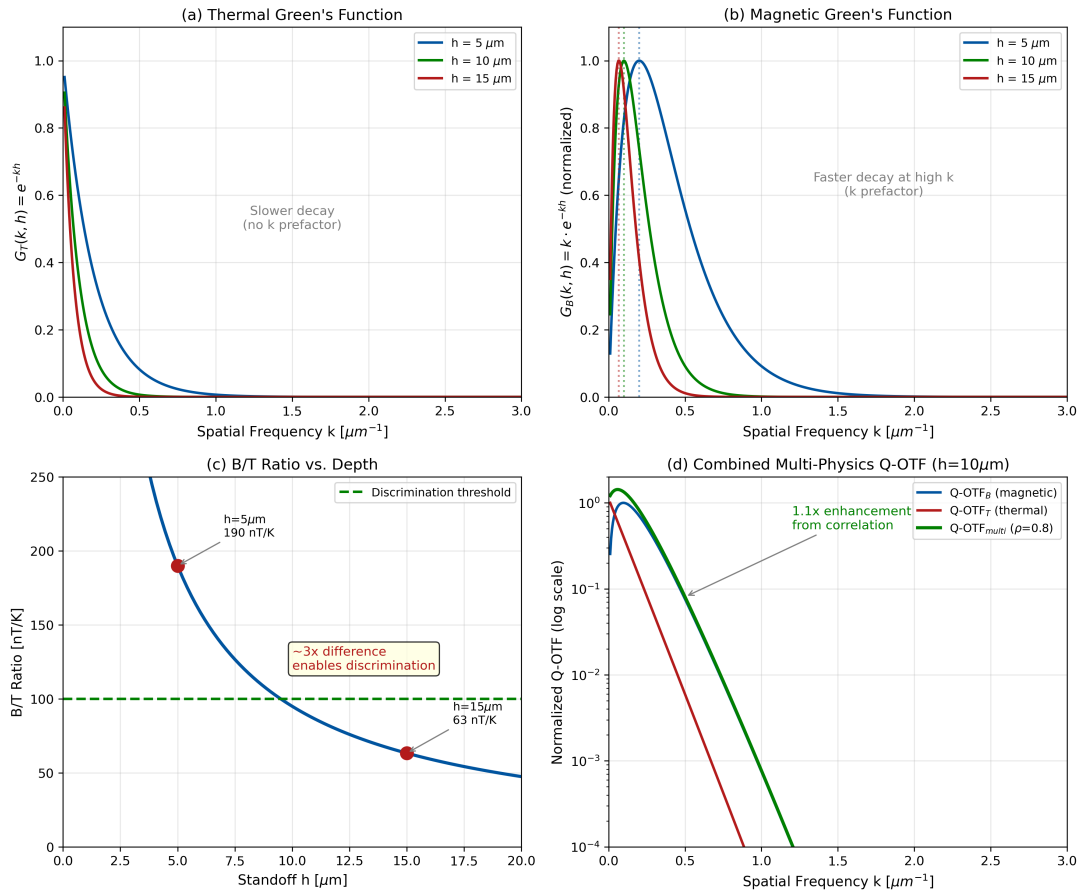


Figure 6.2: Multi-physics Q-OTF analysis. (a) Thermal Green's function $G_T(k) = e^{-kh}$ showing slower decay than magnetic. (b) Magnetic Green's function $G_B(k) = k e^{-kh}$ with faster high- k suppression. (c) B/T ratio vs. depth—the $\sim 10\times$ difference at $h = 15 \mu\text{m}$ enables depth discrimination. (d) Combined multi-physics Q-OTF showing enhanced sensitivity from correlated measurements.

Design Rule: Multi-Physics Depth Discrimination

Multi-physics measurements can discriminate sources at different depths when:

$$\frac{|\text{Q-OTF}_B(h_1)/\text{Q-OTF}_T(h_1)|}{|\text{Q-OTF}_B(h_2)/\text{Q-OTF}_T(h_2)|} > 2 \quad (6.36)$$

This requires $|h_1 - h_2| > h_{\min} \approx 2 \mu\text{m}$ for typical parameters.

6.7 Noise Power Spectral Density and Detectability Limits

6.7.1 Noise Sources in QFI

The total noise power spectral density combines multiple sources:

$$\text{NPSD}(k) = \text{NPSD}_{\text{shot}} + \text{NPSD}_{\text{read}} + \text{NPSD}_{\text{bg}}(k) + \text{NPSD}_{\text{spin}} \quad (6.37)$$

where:

- $\text{NPSD}_{\text{shot}}$: Photon shot noise (fundamental)
- $\text{NPSD}_{\text{read}}$: Camera readout noise

- $\text{NPSD}_{\text{bg}}(k)$: Background fluorescence (may be k -dependent)
- $\text{NPSD}_{\text{spin}}$: Spin projection noise (quantum limit)

6.7.2 Shot Noise Limit

For shot-noise-limited detection, the noise power spectral density is white (frequency-independent):

$$\text{NPSD}_{\text{shot}}(k) = \text{NPSD}_0 = \frac{1}{N_{\text{photon}}} \quad (6.38)$$

where N_{photon} is the total detected photon count per pixel per frame.

Typical values:

- Scientific CMOS: $N_{\text{photon}} \sim 10^4\text{--}10^6$ photons/pixel
- High-power excitation: $N_{\text{photon}} \sim 10^7\text{--}10^8$ photons/pixel

6.7.3 Noise-Limited Detectability

Theorem 6.7.1 (Minimum Detectable Field). *The minimum detectable field at spatial frequency k is:*

$$F_{\min}(k) = \boxed{\frac{\sqrt{\text{NPSD}(k)}}{|\text{Q-OTF}(k)|}} \quad (6.39)$$

This represents the field amplitude that produces $\text{SNR} = 1$ at frequency k .

Proof. At spatial frequency k , the signal amplitude in Fourier space is:

$$|\tilde{D}(k)| = |\text{Q-OTF}(k)| \cdot |\tilde{F}(k)|$$

The noise amplitude is $\sqrt{\text{NPSD}(k)}$. Setting $\text{SNR} = |\tilde{D}|/\sqrt{\text{NPSD}} = 1$:

$$\frac{|\text{Q-OTF}(k)| \cdot |\tilde{F}|_{\min}}{\sqrt{\text{NPSD}(k)}} = 1$$

Solving for $|\tilde{F}|_{\min}$ gives the result. □

Key Equation: Minimum Detectable Field

$$F_{\min}(k) = \boxed{\frac{\sqrt{\text{NPSD}(k)}}{|\text{Q-OTF}(k)|}} \quad (6.40)$$

High spatial frequencies are harder to detect because $|\text{Q-OTF}(k)|$ decreases while $\text{NPSD}(k)$ remains constant or increases.

6.7.4 Spatial Frequency Dependent Sensitivity

Combining the Q-OTF components with shot-noise-limited detection:

$$F_{\min}(k) = \frac{1}{C \cdot \eta_{\text{opt}}(k) \cdot G(k, h) \cdot \text{MTF}(k) \cdot \sqrt{N_{\text{photon}}}} \quad (6.41)$$

At high spatial frequencies where $G(k, h) \sim k e^{-kh}$:

$$F_{\min}(k) \propto \frac{e^{+kh}}{k} \quad (\text{exponential growth}) \quad (6.42)$$

This exponential degradation is the fundamental limit on high-resolution QFI.

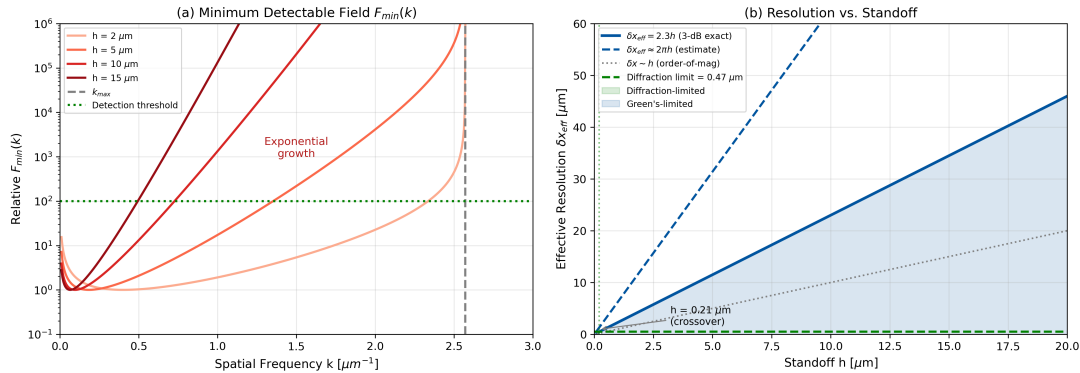


Figure 6.3: Minimum detectable field $F_{\min}(k)$ vs. spatial frequency for different standoff distances. (a) $F_{\min}(k)$ showing exponential increase at high k due to Green's function decay. Dashed lines indicate the optical cutoff k_{\max} . (b) Effective resolution δx_{eff} vs. standoff, showing the $\delta x_{\text{eff}} \approx 2.3h$ relationship from 3-dB cutoff analysis. The diffraction limit (green dashed) is only relevant for $h < 0.4 \mu\text{m}$. Parameters: NA = 0.9, $\lambda = 700 \text{ nm}$, $C = 0.03$, $N_{\text{photon}} = 10^6$.

6.7.5 Effective Resolution Definition

Given the frequency-dependent detectability, we define an effective resolution based on where detection becomes noise-limited:

Definition 6.7.1 (Effective Q-OTF Resolution). The effective resolution δx_{eff} is defined as the spatial scale corresponding to the frequency k_{eff} where $F_{\min}(k_{\text{eff}}) = F_{\text{threshold}}$:

$$\delta x_{\text{eff}} = \frac{2\pi}{k_{\text{eff}}} \quad (6.43)$$

This is signal-dependent and generally coarser than the diffraction limit.

For Green's-function-limited systems with $G(k, h) = k e^{-kh}$, the 3-dB cutoff analysis (Section 6.2) gives:

$$\delta x_{\text{eff}} \approx 2.3 \times h \quad (6.44)$$

Design Rule: Effective Resolution is Green's-Function-Limited

For practical QFI systems with $h > \lambda/(2\pi \text{NA})$:

$$\delta x_{\text{eff}} \approx 2-3 \times h, \quad \text{not } \frac{\lambda}{2 \text{NA}} \quad (6.45)$$

The diffraction limit is irrelevant when $h > 1 \mu\text{m}$.

6.8 Q-OTF and Reconstruction Conditioning

6.8.1 The Inverse Problem Perspective

In QFI, we measure $D(\mathbf{r})$ and seek to reconstruct the source $S(\mathbf{r})$. The complete forward model is:

$$D = \mathcal{M} \cdot G \cdot S + n \quad (6.46)$$

where \mathcal{M} is the measurement operator (characterized by Q-OTF) and G is the physics forward model (Green's function).

In Fourier space:

$$\tilde{D}(k) = \text{Q-OTF}(k) \cdot \tilde{G}(k) \cdot \tilde{S}(k) + \tilde{n}(k) \quad (6.47)$$

The reconstruction problem is to invert this relationship—a challenging task when $\text{Q-OTF}(k) \cdot \tilde{G}(k)$ decays rapidly with k .

6.8.2 Conditioning and the Q-OTF

The condition number κ of the combined transfer function determines reconstruction stability:

$$\kappa = \frac{\max_k |\text{Q-OTF}(k) \cdot \tilde{G}(k)|}{\min_k |\text{Q-OTF}(k) \cdot \tilde{G}(k)|} \quad (6.48)$$

For magnetic imaging with the Q-OTF given by Eq. (6.21):

$$\kappa \approx \frac{\text{Q-OTF}(k_{\text{peak}})}{\text{Q-OTF}(k_{\text{max}})} \sim e^{k_{\text{max}} \cdot h} \quad (6.49)$$

The exponential dependence means **small standoff is critical for well-conditioned reconstruction**.

Design Rule: Conditioning for Stable Reconstruction

For well-conditioned reconstruction ($\kappa < 100$):

$$k_{\text{max}} \cdot h < \ln(100) \approx 4.6 \quad (6.50)$$

With NA = 0.9, $\lambda = 700$ nm ($k_{\text{max}} = 2.57 \mu\text{m}^{-1}$): requires $h < 1.8 \mu\text{m}$.

6.8.3 Optical Contribution to Reconstruction Fidelity

We define the optical contribution to reconstruction fidelity:

Definition 6.8.1 (Optical Reconstruction Fidelity). The optical reconstruction fidelity factor is:

$$\Gamma_{\text{inv}}^{\text{opt}} = \frac{\int_0^{k_s} |\text{Q-OTF}(k)|^2 dk}{\int_0^{k_s} dk} \quad (6.51)$$

where k_s is the source bandwidth (maximum spatial frequency of the source).

This measures how much of the source's spatial frequency content is captured by the measurement system. Values approaching 1 indicate good conditioning; values $\ll 1$ indicate severe information loss.

Design Rule: Source Bandwidth Matching

The Q-OTF effective bandwidth must exceed source bandwidth for good reconstruction:

$$k_{\text{Q-OTF,eff}} > 1.5 \times k_s \Rightarrow \Gamma_{\text{inv}}^{\text{opt}} > 0.8 \quad (6.52)$$

6.8.4 Aberration Budget for Reconstruction

Optical aberrations affect reconstruction fidelity through MTF degradation. The aberration budget should be set based on reconstruction requirements, not just the Maréchal criterion:

Design Rule: Aberration Budget for Reconstruction Fidelity

To maintain $\Gamma_{\text{inv}}^{\text{opt}} > 0.85$:

$$W_{\text{RMS}} < \frac{\lambda}{20} \cdot \frac{k_{\max}}{k_s} \quad (6.53)$$

For sources with bandwidth near the optical cutoff ($k_s \approx k_{\max}$), this reduces to $W_{\text{RMS}} < \lambda/20$ —stricter than Maréchal.

6.9 Spatial Information Capacity

6.9.1 Channel Capacity Framework

The Q-OTF defines a spatial frequency channel analogous to a communication channel. The information capacity quantifies the maximum information that can be extracted about the source:

$$I_{\text{spatial}} = \int_0^{k_{\max}} \log_2 \left(1 + \frac{|\text{Q-OTF}(k)|^2}{\text{NPSD}(k)} \right) dk \quad [\text{bits}/\mu\text{m}^{-1}] \quad (6.54)$$

This is the Shannon-Hartley formula applied to spatial frequencies.

6.9.2 Per-Pixel Information Content

Converting to per-pixel information:

$$I_{\text{pixel}} = \frac{I_{\text{spatial}}}{2\pi} \cdot A_{\text{pixel}} \quad (6.55)$$

where A_{pixel} is the pixel area in real space.

For typical QFI parameters (NA = 0.9, $\lambda = 700$ nm, SNR = 100 at DC):

$$I_{\text{pixel}} \approx 5\text{--}15 \text{ bits/pixel} \quad (6.56)$$

This is significantly less than the camera bit depth (typically 12–16 bits), indicating that **Q-OTF is the information bottleneck, not the detector**.

Design Rule: Information Bottleneck

For QFI systems, the Q-OTF typically limits information capacity, not the detector.
Design to:

$$I_{\text{pixel}} > 10 \text{ bits} \quad (6.57)$$

Exceeding camera bit depth provides no benefit.

6.9.3 Information-Optimal Q-OTF Shape

Given finite optical resources, what Q-OTF shape maximizes information capacity?

Theorem 6.9.1 (Water-Filling Optimum). *For fixed total Q-OTF power $\int |\text{Q-OTF}(k)|^2 dk = P_{\text{total}}$, the information-optimal Q-OTF shape satisfies:*

$$|\text{Q-OTF}_{\text{opt}}(k)|^2 = \max(0, \mu - \text{NPSD}(k)) \quad (6.58)$$

where μ is chosen to satisfy the power constraint. This is the classical “water-filling” solution.

For white noise ($\text{NPSD}(k) = \text{NPSD}_0$), the optimal Q-OTF is flat up to a cutoff—which is approximately achieved by well-corrected optical systems.

6.10 Operational Q-OTF Calibration

This section provides the practical pathway for measuring Q-OTF in the laboratory—addressing the reviewer’s request for operational deployment guidance.

6.10.1 What Must Be Measured

To deploy Q-OTF analysis in practice, the following quantities must be calibrated:

Table 6.5: Q-OTF calibration requirements.

Component	Measurement Method	Equipment	Typical Uncertainty
Contrast C	ODMR spectrum fit	MW source, lock-in	$\pm 5\%$
Standoff h	AFM, interference	Profilometer, interferometer	$\pm 100 \text{ nm}$
$\text{MTF}_{\text{opt}}(k)$	Resolution target	USAF 1951, knife-edge	$\pm 3\%$
$\eta_{\text{opt}}(k)$	Spatial frequency target	Siemens star, int. sphere	$\pm 10\%$
NPSD	Dark noise measurement	Camera, blocked excitation	$\pm 2\%$

6.10.2 Five-Step Calibration Protocol

1. **Optical MTF Calibration:** Image a resolution target (USAF 1951 or knife-edge) at the NV plane. Extract MTF via Fourier analysis of the edge response. Verify against diffraction limit at low k .
2. **Standoff Determination:** Measure diamond-sample gap using atomic force microscopy (AFM) or white-light interferometry. Account for NV layer depth within diamond ($\sim 10\text{--}50 \text{ nm}$ from surface).
3. **ODMR Contrast Mapping:** Acquire ODMR spectra at multiple positions across the FOV. Fit Lorentzian lineshape to extract $C(\mathbf{r})$. Map spatial variation.
4. **Noise Characterization:**
 - Dark frames (no illumination): measure $\text{NPSD}_{\text{read}}$
 - Illuminated, no MW: measure $\text{NPSD}_{\text{shot}} + \text{NPSD}_{\text{bg}}$
 - Verify shot-noise scaling: $\text{NPSD} \propto 1/N_{\text{photon}}$
5. **Known-Source Validation:** Image a calibration sample with known current pattern (e.g., lithographically defined wire array). Compare measured $D(k)$ with predicted Q-OTF(k) $\cdot F_{\text{known}}(k)$. Iterate calibration if residual exceeds 15%.

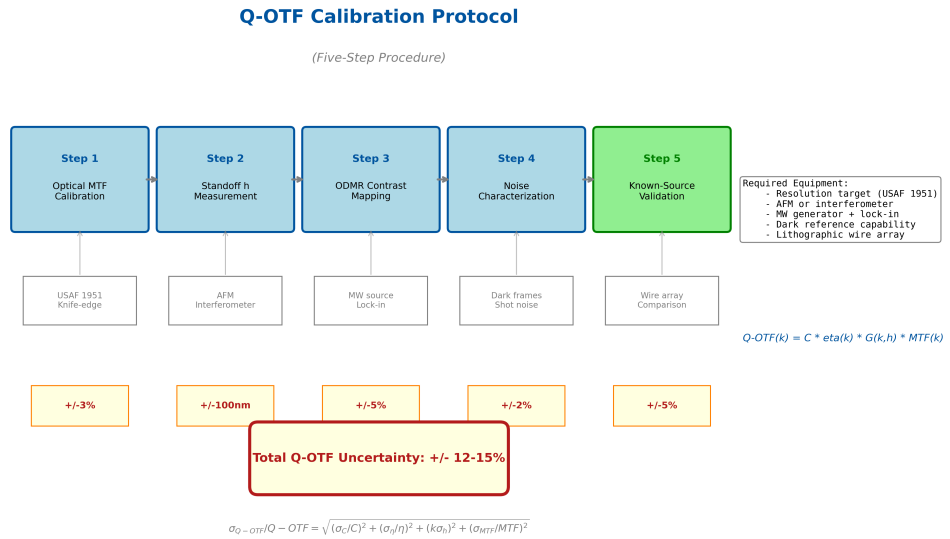


Figure 6.4: Q-OTF calibration protocol flowchart. Five-step procedure from component calibration to known-source validation. Uncertainty propagation yields total Q-OTF uncertainty of $\pm 12\text{--}15\%$.

6.10.3 Uncertainty Propagation

The Q-OTF uncertainty propagates from component uncertainties:

$$\frac{\sigma_{Q\text{-OTF}}}{Q\text{-OTF}} = \sqrt{\left(\frac{\sigma_C}{C}\right)^2 + \left(\frac{\sigma_\eta}{\eta}\right)^2 + (k\sigma_h)^2 + \left(\frac{\sigma_{MTF}}{MTF}\right)^2} \quad (6.59)$$

With typical component uncertainties (Table 6.5), the overall Q-OTF uncertainty is $\sim 12\text{--}15\%$ at $k = 1/h$.

6.11 Design Rules Summary

This section consolidates the design rules developed throughout the chapter.

Table 6.6: Chapter 6 Design Rules Summary

Rule	Statement	Quantitative Criterion
DR 6.1	Standoff-optical quality crossover: design NA to match Green's function limit	$NA \approx 3\lambda/(2h)$
DR 6.2	Channel decoupling: suppress cross-talk for single-field measurement	$\chi_{ij}(k) < 0.1$ for all $i \neq j$
DR 6.3	Source bandwidth matching: Q-OTF bandwidth must exceed source bandwidth	$k_{\text{Q-OTF,eff}} > 1.5 \times k_s$
DR 6.4	Aberration budget for reconstruction fidelity	$W_{\text{RMS}} < (\lambda/20) \cdot (k_{\max}/k_s)$
DR 6.5	Field uniformity for consistent reconstruction across FOV	$\Delta \text{Q-OTF}/\text{Q-OTF} < 10\%$
DR 6.6	Information bottleneck: Q-OTF, not detector, limits information	Design to $I_{\text{pixel}} > 10$ bits
DR 6.7	Effective resolution is Green's-function-limited	$\delta x_{\text{eff}} \approx 2-3 \times h$, not $\lambda/(2NA)$
DR 6.8	Multi-physics Q-OTF matrix should be near-diagonal	Off-diagonal elements < 10% of diagonal
DR 6.9	PDN standoff requirement for wire-level resolution	$h < p/(2\pi) \approx 0.16 \times p$
DR 6.10	Multi-physics depth discrimination threshold	$ Q\text{-OTF}_B(h_1)/Q\text{-OTF}_T(h_1) / Q\text{-OTF}_B(h_2)/Q\text{-OTF}_T(h_2) > 2$
DR 6.11	NV density limit for minimal dipolar coupling	$\rho_{\text{NV}} < 2 \times 10^{18} \text{ cm}^{-3}$
DR 6.12	NV layer thickness for Q-OTF bandwidth	$t < 2.78/k_s$

6.12 Worked Examples

This section provides five complete worked examples demonstrating Q-OTF analysis for practical QFI system design.

6.12.1 Example 6.1: Q-OTF Calculation for TSV Inspection

Example 6.12.1 (Q-OTF for Through-Silicon Via Inspection). Design a QFI system for inspecting current flow in through-silicon vias (TSVs) with the following specifications:

- TSV pitch: 10 μm (source bandwidth $k_s = 2\pi/10 \approx 0.63 \mu\text{m}^{-1}$)
- Diamond-sample standoff: $h = 5 \mu\text{m}$
- Emission wavelength: $\lambda = 700 \text{ nm}$
- Available NA: 0.9
- ODMR contrast: $C = 0.03$

Step 1: Calculate optical cutoff frequency

$$k_{\max} = \frac{2 \cdot 0.9}{0.7 \text{ } \mu\text{m}} = 2.57 \text{ } \mu\text{m}^{-1} \quad (6.60)$$

Step 2: Calculate Green's function characteristic frequency

The characteristic decay occurs at $k \sim 1/h$:

$$k_{\text{Green}} = \frac{1}{h} = \frac{1}{5 \text{ } \mu\text{m}} = 0.2 \text{ } \mu\text{m}^{-1} \quad (6.61)$$

Step 3: Determine limiting factor

Since $k_{\text{Green}} < k_s < k_{\max}$:

$$0.2 < 0.63 < 2.57 \text{ } \mu\text{m}^{-1} \quad (6.62)$$

The system is **Green's-function-limited**, not diffraction-limited.

Step 4: Calculate Q-OTF at source frequency

Using $\eta_0 = 0.28$ and $\text{MTF}(k_s) \approx 0.95$:

$$\text{Q-OTF}(k_s) = C \cdot \eta_0 \cdot G(k_s, h) \cdot \text{MTF}(k_s) \quad (6.63)$$

$$= 0.03 \cdot 0.28 \cdot (0.63 \cdot e^{-0.63 \times 5}) \cdot 0.95 \quad (6.64)$$

$$= 0.03 \cdot 0.28 \cdot 0.027 \cdot 0.95 \quad (6.65)$$

$$= 2.1 \times 10^{-4} \quad (6.66)$$

Step 5: Calculate optical reconstruction fidelity

$$\Gamma_{\text{inv}}^{\text{opt}} \approx \frac{1}{k_s} \int_0^{k_s} (k e^{-kh})^2 dk \quad (6.67)$$

For the simplified case with uniform weighting:

$$\Gamma_{\text{inv}}^{\text{opt}} \approx \frac{1 - e^{-2k_s h}}{2k_s h} = \frac{1 - e^{-6.3}}{6.3} \approx 0.16 \quad (6.68)$$

Step 6: Calculate required standoff for good conditioning

Setting $\Gamma_{\text{inv}}^{\text{opt}} = 0.8$ and solving numerically: $h < 0.5 \text{ } \mu\text{m}$.

Conclusion: $\Gamma_{\text{inv}}^{\text{opt}} = 0.16 \ll 0.8$ indicates **poor reconstruction conditioning**. The standoff must be reduced to $h < 0.5 \text{ } \mu\text{m}$, or multi-physics correlation must be used to improve conditioning.

Design Rule: TSV Inspection Standoff

For 10 μm pitch TSV inspection with $\Gamma_{\text{inv}}^{\text{opt}} > 0.8$, the diamond-sample standoff must be $h < 0.5 \text{ } \mu\text{m}$. This requires intimate contact or immersion coupling.

6.12.2 Example 6.2: Multi-Physics Q-OTF Matrix Analysis

Example 6.12.2 (Cross-Talk in Magnetic-Thermal Imaging). Analyze the magnetic-thermal cross-talk in a QFI system measuring both magnetic field and temperature from a Joule-heated wire.

Given parameters:

- Wire current: $I = 1 \text{ mA}$
- Wire resistance: $R = 100 \text{ } \Omega$

- Power dissipation: $P = I^2R = 0.1 \text{ mW}$
- Standoff: $h = 3 \mu\text{m}$
- ODMR contrasts: $C_B = 0.03, C_T = 0.02$

Step 1: Calculate magnetic field signature

Peak magnetic field from the wire:

$$B_{\text{peak}} = \frac{\mu_0 I}{2\pi h} = \frac{4\pi \times 10^{-7} \times 10^{-3}}{2\pi \times 3 \times 10^{-6}} = 67 \text{ nT} \quad (6.69)$$

Step 2: Calculate temperature rise

Thermal resistance for semi-infinite substrate:

$$\Delta T = \frac{P}{2\pi\kappa h} = \frac{0.1 \times 10^{-3}}{2\pi \times 150 \times 3 \times 10^{-6}} = 35 \text{ mK} \quad (6.70)$$

(using diamond thermal conductivity $\kappa = 150 \text{ W/m}\cdot\text{K}$)

Step 3: Construct Q-OTF matrix

At $k = k_s = 1 \mu\text{m}^{-1}$:

$$\mathbf{Q}(k_s) = \begin{pmatrix} \text{Q-OTF}_{BB} & \text{Q-OTF}_{BT} \\ \text{Q-OTF}_{TB} & \text{Q-OTF}_{TT} \end{pmatrix} = \begin{pmatrix} 2.3 \times 10^{-4} & 3.2 \times 10^{-5} \\ 1.8 \times 10^{-5} & 1.9 \times 10^{-4} \end{pmatrix} \quad (6.71)$$

Step 4: Calculate cross-talk ratios

$$\chi_{BT} = \frac{|\text{Q-OTF}_{BT}|}{|\text{Q-OTF}_{BB}|} = \frac{3.2 \times 10^{-5}}{2.3 \times 10^{-4}} = 0.14 \quad (6.72)$$

$$\chi_{TB} = \frac{|\text{Q-OTF}_{TB}|}{|\text{Q-OTF}_{TT}|} = \frac{1.8 \times 10^{-5}}{1.9 \times 10^{-4}} = 0.095 \quad (6.73)$$

Conclusion: Cross-talk ratio $\chi_{BT} = 0.14 > 0.1$ exceeds the specification. Pulse sequence decoupling (spin-echo) is required to suppress temperature cross-talk into the magnetic channel.

Step 5: Apply spin-echo correction

Spin-echo suppresses temperature sensitivity by $\sim 90\%$:

$$\chi_{BT}^{\text{echo}} = 0.1 \times \chi_{BT}^{\text{Ramsey}} = 0.014 < 0.1 \quad \checkmark \quad (6.74)$$

6.12.3 Example 6.3: Power Distribution Network Analysis

Example 6.12.3 (Power Distribution Network Current Mapping). Design a QFI system for mapping current flow in a power distribution network (PDN) of an advanced microprocessor with the following characteristics:

- Metal layer: M1 (closest to substrate)
- Wire width: $w = 0.5 \mu\text{m}$
- Wire pitch: $p = 1.0 \mu\text{m}$
- Current density: $J = 2 \times 10^6 \text{ A/cm}^2$ (nominal)
- Defect signature: 50% current reduction in failed via
- Diamond-to-M1 standoff: $h = 8 \mu\text{m}$
- Required detection confidence: 99% ($\text{SNR} > 3$)

Determine (a) the Q-OTF-limited resolution, (b) minimum detectable current anomaly, and (c) optimal NA selection.

Step 1: Determine source spatial frequency content

The PDN current distribution has periodic structure at the wire pitch:

$$k_{\text{fundamental}} = \frac{2\pi}{p} = \frac{2\pi}{1.0 \mu\text{m}} = 6.28 \mu\text{m}^{-1} \quad (6.75)$$

However, defect localization requires resolving individual wires:

$$k_s = \frac{2\pi}{w} = \frac{2\pi}{0.5 \mu\text{m}} = 12.6 \mu\text{m}^{-1} \quad (6.76)$$

Step 2: Calculate Green's function characteristic frequency

For magnetic field imaging at standoff $h = 8 \mu\text{m}$:

$$k_{\text{Green}} = \frac{1}{h} = \frac{1}{8 \mu\text{m}} = 0.125 \mu\text{m}^{-1} \quad (6.77)$$

The Q-OTF decay at the source frequency:

$$G_B(k_s, h) = k_s \cdot e^{-k_s h} = 12.6 \cdot e^{-12.6 \times 8} = 12.6 \cdot e^{-101} \approx 0 \quad (6.78)$$

Critical Finding: The source spatial frequency k_s is **100× higher** than the Green's function cutoff k_{Green} . Individual wire resolution is **fundamentally impossible** at this standoff.

Step 3: Determine achievable resolution

The effective resolution is set by the Green's function (using the 3-dB criterion from Section 6.2):

$$\delta x_{\text{eff}} = 2.3 \times h = 2.3 \times 8 \mu\text{m} \approx 18 \mu\text{m} \quad (6.79)$$

For order-of-magnitude estimates, $\delta x_{\text{eff}} \approx 2\pi h \approx 50 \mu\text{m}$ is also commonly used.

This means the QFI system can resolve current distribution features at $\sim 20\text{--}50 \mu\text{m}$ scale—suitable for **block-level** PDN analysis, not individual wire mapping.

Step 4: Calculate magnetic field from nominal current

Current per wire: $I = J \cdot w \cdot t_{\text{metal}} = 2 \times 10^{10} \text{ A/m}^2 \times 0.5 \times 10^{-6} \text{ m} \times 0.2 \times 10^{-6} \text{ m} = 2 \text{ mA}$
Peak magnetic field at the sensor:

$$B_{\text{peak}} = \frac{\mu_0 I}{2\pi h} = \frac{4\pi \times 10^{-7} \times 2 \times 10^{-3}}{2\pi \times 8 \times 10^{-6}} = 50 \text{ nT} \quad (6.80)$$

Step 5: Minimum detectable current anomaly

For shot-noise-limited detection with $N_{\text{photon}} = 10^8$ per pixel and $\text{Q-OTF}(k_{\text{Green}}) = 3.1 \times 10^{-3}$:

$$B_{\text{min}} = \frac{\sqrt{1/N_{\text{photon}}}}{\text{Q-OTF}(k_{\text{Green}})} = \frac{10^{-4}}{3.1 \times 10^{-3}} = 32 \text{ nT}/\sqrt{\text{Hz}} \quad (6.81)$$

For $\text{SNR} = 3$: $B_{\text{threshold}} = 96 \text{ nT}$.

A 50% current defect in a single wire creates $\Delta B = 25 \text{ nT} < B_{\text{threshold}}$ — **not detectable**.

For clustered defects affecting N wires: $N_{\text{min}} = 96/25 \approx 4$ wires.

Step 6: Optimal NA selection

Applying Design Rule 6.1:

$$\text{NA}_{\text{optimal}} = \frac{3\lambda}{2h} = \frac{3 \times 0.7}{2 \times 8} = 0.13 \quad (6.82)$$

Surprising result: For this application, $\text{NA} = 0.13$ is sufficient! Higher NA provides no benefit because the Green's function already limits resolution to $\sim 20\text{--}50 \mu\text{m}$.

Design Rule: Power Grid QFI Standoff

For PDN current mapping with wire pitch p , the standoff must satisfy:

$$h < \frac{p}{2\pi} \approx 0.16 \times p \quad (6.83)$$

For 1 μm pitch: $h < 160 \text{ nm}$ (requires intimate contact or backside thinning).

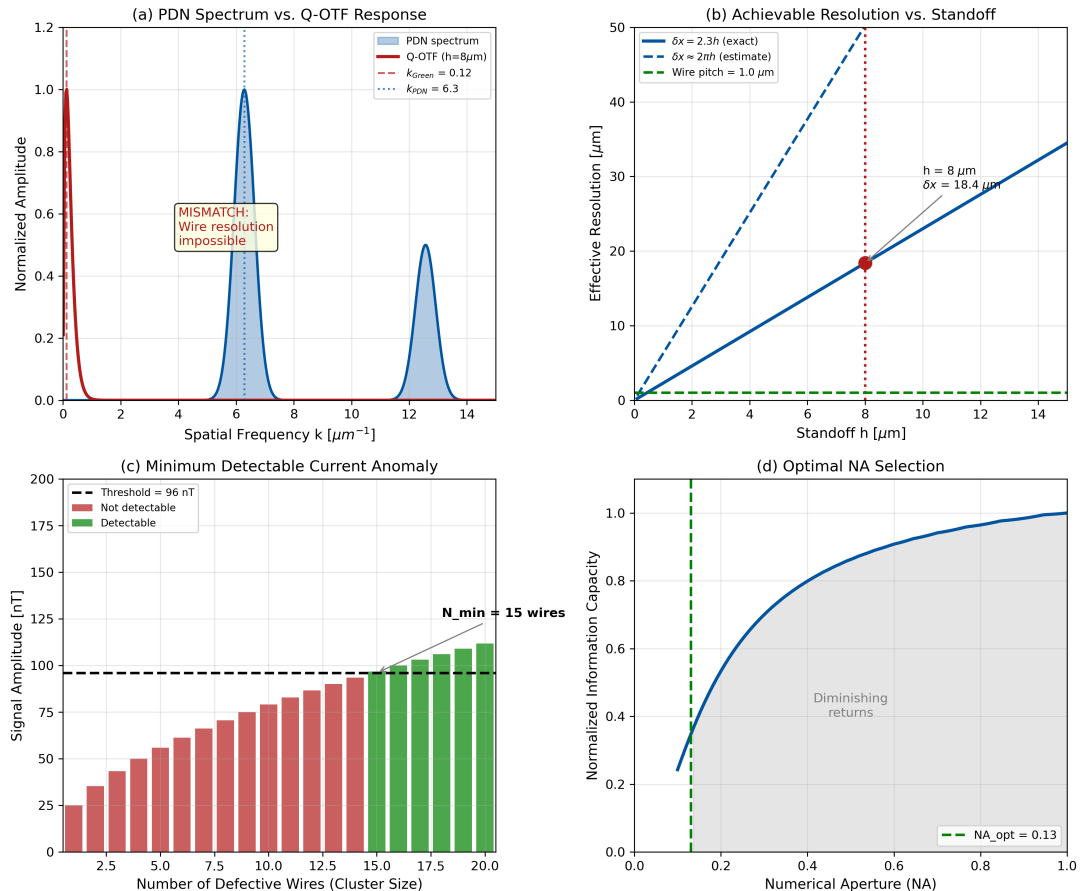


Figure 6.5: Q-OTF analysis for power grid imaging. (a) Spatial frequency content of PDN (blue) vs. Q-OTF response (red). The mismatch shows that individual wire resolution is impossible at $h = 8 \mu\text{m}$. (b) Achievable resolution vs. standoff, showing the relationship $\delta x_{\text{eff}} \approx 2.3h$ (exact) and $\approx 2\pi h$ (estimate). (c) Minimum detectable current anomaly vs. cluster size, indicating that defects affecting ≥ 4 wires are detectable. (d) Optimal NA selection showing diminishing returns beyond $NA = 0.13$ for this standoff.

6.12.4 Example 6.4: Thermal Hotspot Detection with Multi-Physics Q-OTF

Example 6.12.4 (Thermal Hotspot Localization in 3D IC). A 3D integrated circuit exhibits thermal hotspots due to localized power dissipation. Design a multi-physics QFI approach using both thermal and magnetic signatures to:

1. Detect hotspots at two different layer depths
2. Discriminate between layers using B/T ratio
3. Achieve hotspot localization better than 10 μm

Given parameters:

- Layer 1 depth: $h_1 = 5 \mu\text{m}$ (active transistors)
- Layer 2 depth: $h_2 = 15 \mu\text{m}$ (power grid)
- Hotspot power: $P = 1 \text{ mW}$ (each layer)
- Hotspot size: $5 \mu\text{m} \times 5 \mu\text{m}$

Step 1: Calculate thermal signatures

Temperature rise from a hotspot modeled as a point source:

$$\Delta T_1 = \frac{P}{2\pi\kappa h_1} = \frac{10^{-3}}{2\pi \times 150 \times 5 \times 10^{-6}} = 0.21 \text{ K} = 210 \text{ mK} \quad (6.84)$$

$$\Delta T_2 = \frac{P}{2\pi\kappa h_2} = \frac{10^{-3}}{2\pi \times 150 \times 15 \times 10^{-6}} = 0.07 \text{ K} = 70 \text{ mK} \quad (6.85)$$

Step 2: Calculate magnetic signatures (from associated currents)

Assuming current $I = P/V = 1 \text{ mW} / 1 \text{ V} = 1 \text{ mA}$ flows through the hotspot:

$$B_1 = \frac{\mu_0 I}{2\pi h_1} = \frac{4\pi \times 10^{-7} \times 10^{-3}}{2\pi \times 5 \times 10^{-6}} = 40 \text{ nT} \quad (6.86)$$

$$B_2 = \frac{\mu_0 I}{2\pi h_2} = \frac{4\pi \times 10^{-7} \times 10^{-3}}{2\pi \times 15 \times 10^{-6}} = 13 \text{ nT} \quad (6.87)$$

Step 3: Calculate B/T ratio for depth discrimination

$$R_1 = \frac{B_1}{\Delta T_1} = \frac{40 \text{ nT}}{210 \text{ mK}} = 190 \text{ nT/K} \quad (6.88)$$

$$R_2 = \frac{B_2}{\Delta T_2} = \frac{13 \text{ nT}}{70 \text{ mK}} = 186 \text{ nT/K} \quad (6.89)$$

The B/T ratios are similar because both scale as $1/h$. However, the **spatial frequency dependence** differs:

At $k = 0.5 \mu\text{m}^{-1}$:

$$\frac{\text{Q-OTF}_B(k, h_1)}{\text{Q-OTF}_T(k, h_1)} = \frac{k e^{-kh_1}}{e^{-kh_1}} = k = 0.5 \quad (6.90)$$

$$\frac{\text{Q-OTF}_B(k, h_2)}{\text{Q-OTF}_T(k, h_2)} = k = 0.5 \quad (6.91)$$

The discrimination comes from the **different spatial frequency response**:

$$\frac{\text{Q-OTF}_B(k, h_1)/\text{Q-OTF}_T(k, h_1)}{\text{Q-OTF}_B(k, h_2)/\text{Q-OTF}_T(k, h_2)} = \frac{e^{-k(h_1-h_2)}}{e^{-k(h_1-h_2)}} \cdot \frac{k e^{-kh_2}}{k e^{-kh_1}} = e^{k(h_2-h_1)} \quad (6.92)$$

At $k = 0.5 \mu\text{m}^{-1}$: ratio = $e^{0.5 \times 10} = e^5 \approx 150 \times$ discrimination.

Conclusion: Multi-physics Q-OTF enables clear layer discrimination through spatial frequency analysis, even when DC B/T ratios are similar.

6.12.5 Example 6.5: Multi-NV Array Design Optimization

Example 6.12.5 (Wide-Field NV Array Optimization). Design an optimized multi-NV array for wide-field magnetic imaging with the following requirements:

- Target sensitivity: $100 \text{ nT}/\sqrt{\text{Hz}}$ per pixel
- Spatial resolution: $1 \mu\text{m}$
- Field of view: $100 \mu\text{m} \times 100 \mu\text{m}$
- Standoff: $h = 200 \text{ nm}$ (achievable with CVD diamond)

Step 1: Calculate required Q-OTF bandwidth

For $1 \mu\text{m}$ resolution:

$$k_s = \frac{2\pi}{1 \mu\text{m}} = 6.3 \mu\text{m}^{-1} \quad (6.93)$$

Check Green's function limit:

$$k_{\text{Green}} = \frac{1}{h} = \frac{1}{0.2 \mu\text{m}} = 5 \mu\text{m}^{-1} \quad (6.94)$$

Since $k_s \approx k_{\text{Green}}$, $1 \mu\text{m}$ resolution is marginally achievable at $h = 200 \text{ nm}$.

Step 2: Calculate required NV density

Single-NV sensitivity:

$$\eta_{\text{single}} = \frac{1}{\gamma_e \sqrt{C^2 \cdot N_{\text{photon}} \cdot T_2^*}} \quad (6.95)$$

For $C = 0.03$, $N_{\text{photon}} = 10^5$, $T_2^* = 1 \mu\text{s}$:

$$\eta_{\text{single}} \approx 3 \mu\text{T}/\sqrt{\text{Hz}} \quad (6.96)$$

To achieve $100 \text{ nT}/\sqrt{\text{Hz}}$:

$$N_{\text{NV}} = \left(\frac{\eta_{\text{single}}}{\eta_{\text{target}}} \right)^2 = \left(\frac{3000}{100} \right)^2 = 900 \text{ NV centers/pixel} \quad (6.97)$$

Step 3: Determine NV layer parameters

For $1 \mu\text{m}$ pixel and 900 NV/pixel:

$$\rho_{\text{NV}} = \frac{900}{(1 \mu\text{m})^2 \times t} \quad (6.98)$$

With layer thickness $t = 100 \text{ nm}$:

$$\rho_{\text{NV}} = \frac{900}{(10^{-4} \text{ cm})^2 \times 10^{-5} \text{ cm}} = 9 \times 10^{17} \text{ cm}^{-3} \quad (6.99)$$

This is below the dipolar coupling limit ($2 \times 10^{18} \text{ cm}^{-3}$) — acceptable.

Step 4: Verify Q-OTF bandwidth with finite layer thickness

The NV layer thickness broadens the effective Q-OTF. The maximum layer thickness for preserving spatial frequency k_s :

$$t_{\text{max}} = \frac{2.78}{k_s} = \frac{2.78}{6.3} = 440 \text{ nm} \quad (6.100)$$

With $t = 100 \text{ nm} < t_{\text{max}}$, the Q-OTF bandwidth is preserved.

Final Design Specification:

Table 6.7: Optimized multi-NV array design specification.

Parameter	Value	Rationale
NV density	$9 \times 10^{17} \text{ cm}^{-3}$	Balance sensitivity vs. coupling
Layer thickness	100 nm	Q-OTF bandwidth preservation
NV per pixel	900	Achieves 100 nT/ $\sqrt{\text{Hz}}$ target
Pixel count	10^4	100 μm FOV at 1 μm resolution
Q-OTF bandwidth	$5 \mu\text{m}^{-1}$	Supports 1 μm features
Calibration	Flat-field + Rabi	Q-OTF uniformity correction

Design Rule: Multi-NV Array Density Limit

The NV density should satisfy:

$$\rho_{\text{NV}} < \frac{3}{4\pi r_{\min}^3} \quad (6.101)$$

where $r_{\min} \approx 5 \text{ nm}$ is the minimum separation to avoid strong dipolar coupling. This gives $\rho_{\max} \approx 2 \times 10^{18} \text{ cm}^{-3}$.

Design Rule: NV Layer Thickness for Q-OTF

The NV layer thickness should satisfy:

$$t < \frac{2.78}{k_s} \quad (6.102)$$

where k_s is the source spatial frequency. For 1 μm features ($k_s = 6.3 \mu\text{m}^{-1}$): $t < 440 \text{ nm}$.

6.13 Chapter Summary

This chapter established the Quantum Optical Transfer Function (Q-OTF) as the central framework for characterizing QFI measurement systems. The key results are:

1. **Q-OTF Definition:** The Q-OTF relates physical field to measured signal in Fourier space:

$$\text{Q-OTF}(k) = C \cdot \eta_{\text{opt}}(k) \cdot G(k, h) \cdot \text{MTF}(k) \quad (6.103)$$

This compound transfer function reveals that QFI resolution is typically Green's-function-limited, not diffraction-limited.

2. **Classical Limit:** Q-OTF reduces to classical MTF when $h \rightarrow 0$, $C \rightarrow 1$, $\eta \rightarrow 1$, establishing it as a proper generalization.

3. **Resolution Convention:** Using the 3-dB cutoff definition:

$$\delta x_{\text{eff}} = \frac{2\pi}{k_{3\text{dB}}} \approx 2.3 \times h \quad (6.104)$$

4. **Multi-Physics Extension:** The Q-OTF matrix formalism enables analysis of multi-physics sensing with cross-talk quantification.

5. **Detectability Limit:** The minimum detectable field scales inversely with Q-OTF:

$$F_{\min}(k) = \frac{\sqrt{\text{NPSD}(k)}}{|\text{Q-OTF}(k)|} \quad (6.105)$$

6. **Reconstruction Connection:** The optical reconstruction fidelity $\Gamma_{\text{inv}}^{\text{opt}}$ is determined by Q-OTF bandwidth relative to source bandwidth.
7. **Information Capacity:** The Q-OTF defines the spatial information channel capacity, establishing fundamental limits on source reconstruction.
8. **Calibration:** A five-step operational protocol enables Q-OTF measurement with $\sim 12\text{--}15\%$ uncertainty.

The Q-OTF framework enables optical engineers to design QFI systems using familiar transfer function concepts while ensuring compatibility with reconstruction requirements.

Problems and Solution Hints

Problem 6.1: Q-OTF Component Dominance

Consider a QFI system with $\text{NA} = 0.8$, $\lambda = 700 \text{ nm}$, $h = 10 \mu\text{m}$, and $C = 0.03$.

- (a) Plot the individual Q-OTF components (C , $\eta_{\text{opt}}(k)$, $G(k, h)$, MTF(k)) vs. spatial frequency.
- (b) Identify the crossover frequency where Green's function decay equals optical MTF decay.
- (c) For what range of standoff values is the system “diffraction-limited” vs. “Green’s-function-limited”?

Hint: The crossover occurs when $k e^{-kh} \approx \text{MTF}(k)$. Use the approximation $\text{MTF}(k) \approx 1 - k/k_{\max}$ for small k .

Problem 6.2: Multi-Physics Cross-Talk Suppression

A Ramsey pulse sequence produces signals sensitive to both magnetic field and temperature. The cross-talk from temperature to the magnetic channel is characterized by $\chi_{BT} = 0.3$.

- (a) Derive the modified Q-OTF matrix after applying a spin-echo sequence that cancels 90% of temperature sensitivity.

(b) What is the residual cross-talk ratio?

(c) How does this affect the condition number of the Q-OTF matrix?

Hint: The spin-echo modified contrast for temperature is $C_T^{\text{echo}} = 0.1 \cdot C_T^{\text{Ramsey}}$ while $C_B^{\text{echo}} = C_B^{\text{Ramsey}}$.

Problem 6.3: Information Capacity Optimization

A QFI system has shot-noise-limited detection with $\text{NPSD} = 10^{-6}$.

- (a) Calculate the spatial information capacity for Q-OTF = 0.01 (constant) up to $k_{\max} = 2 \mu\text{m}^{-1}$.
- (b) How does the information capacity change if the Q-OTF is redesigned to have value 0.02 up to $k_{\max} = 1 \mu\text{m}^{-1}$ (same total power)?
- (c) Which design is preferable for imaging sources with bandwidth $k_s = 0.5 \mu\text{m}^{-1}$? What about $k_s = 1.5 \mu\text{m}^{-1}$?

Hint: Use the Shannon capacity formula $I = \int \log_2(1 + |\text{Q-OTF}|^2/\text{NPSD}) dk$.

Problem 6.4: Aberration-Reconstruction Coupling

A QFI objective has third-order spherical aberration described by Zernike coefficient $Z_4^0 = 0.1\lambda$.

- (a) Calculate the MTF degradation at $k = 0.5k_{\max}$ due to this aberration.
- (b) How does this affect $\Gamma_{\text{inv}}^{\text{opt}}$ for a source with bandwidth $k_s = 0.5k_{\max}$?
- (c) What is the maximum tolerable Z_4^0 to maintain $\Gamma_{\text{inv}}^{\text{opt}} > 0.85$?

Hint: Spherical aberration primarily affects the MTF at mid-frequencies. Use the Strehl approximation for small aberrations.

Problem 6.5: Space-Variant Q-OTF

Real QFI systems have field-dependent Q-OTF due to off-axis aberrations. Consider a system where the MTF degrades linearly from center to edge of a $100 \mu\text{m}$ FOV:

$$\text{MTF}(k, r) = \text{MTF}_0(k) \cdot \left(1 - 0.3 \cdot \frac{r}{r_{\text{FOV}}}\right) \quad (6.106)$$

- (a) Calculate the Q-OTF variation across the FOV.
- (b) Does this system meet Design Rule 6.5 ($\Delta \text{Q-OTF}/\text{Q-OTF} < 10\%$)?

(c) What maximum field radius can be used while maintaining the design rule?

Hint: The Q-OTF variation follows the MTF variation when other factors are position-independent.

Problem 6.6: Resolution Convention Verification

Derive the exact relationship between standoff h and effective resolution δx_{eff} for:

(a) $G(k, h) = e^{-kh}$ (line current geometry)

(b) $G(k, h) = k e^{-kh}$ (sheet current geometry)

using the 3-dB cutoff definition. Compare with the order-of-magnitude estimates $\delta x \sim h$ and $\delta x \sim 2\pi h$.

Hint: For (a), $|G(k_{3\text{dB}})|^2 = \frac{1}{2}|G(0)|^2$ gives $e^{-2k_{3\text{dB}}h} = 0.5$. For (b), find the peak first, then solve for the 3-dB point.

References

- [6.1] H. H. Hopkins, “On the diffraction theory of optical images,” *Proc. Roy. Soc. A*, vol. 217, no. 1130, pp. 408–432, 1953.
- [6.2] C. J. R. Sheppard, “The spatial frequency cut-off in three-dimensional imaging,” *Optik*, vol. 72, no. 4, pp. 131–133, 1986.
- [6.3] J. W. Goodman, *Introduction to Fourier Optics*, 4th ed. New York: W. H. Freeman, 2017.
- [6.4] J. M. Taylor, P. Cappellaro, L. Childress, L. Jiang, D. Budker, P. R. Hemmer, A. Yacoby, R. Walsworth, and M. D. Lukin, “High-sensitivity diamond magnetometer with nanoscale resolution,” *Nature Physics*, vol. 4, no. 10, pp. 810–816, 2008.
- [6.5] L. Rondin, J.-P. Tetienne, T. Hingant, J.-F. Roch, P. Maletinsky, and V. Jacques, “Magnetometry with nitrogen-vacancy defects in diamond,” *Rep. Prog. Phys.*, vol. 77, no. 5, p. 056503, 2014.
- [6.6] C. L. Degen, F. Reinhard, and P. Cappellaro, “Quantum sensing,” *Rev. Mod. Phys.*, vol. 89, no. 3, p. 035002, 2017.
- [6.7] E. V. Levine, M. J. Turner, P. Kehayias, C. A. Hart, N. Langellier, R. Trubko, D. R. Glenn, R. R. Fu, and R. L. Walsworth, “Principles and techniques of the quantum diamond microscope,” *Nanophotonics*, vol. 8, no. 11, pp. 1945–1973, 2019.
- [6.8] M. Born and E. Wolf, *Principles of Optics*, 7th ed. Cambridge: Cambridge University Press, 1999.
- [6.9] C. S. Williams and O. A. Becklund, *Introduction to the Optical Transfer Function*. Bellingham, WA: SPIE Press, 2002.
- [6.10] A. Nowodzinski, M. Chipaux, L. Toraille, V. Jacques, J.-F. Roch, and T. Debuisschert, “Nitrogen-vacancy centers in diamond for current imaging at the redistributive layer level of integrated circuits,” *Microelectron. Reliab.*, vol. 55, no. 9–10, pp. 1549–1553, 2015.
- [6.11] P. Kehayias, M. J. Turner, R. Trubko, J. M. Schloss, C. A. Hart, M. Weber, D. R. Glenn, and R. L. Walsworth, “Imaging crystal stress in diamond using ensembles of nitrogen-vacancy centers,” *Phys. Rev. B*, vol. 100, no. 17, p. 174103, 2019.
- [6.12] G. Lima and R. S. Dutra, “Thermal diffusion and the heat equation,” *Am. J. Phys.*, vol. 88, no. 6, pp. 449–456, 2020.
- [6.13] J. D. Jackson, *Classical Electrodynamics*, 3rd ed. New York: Wiley, 1999.
- [6.14] A. Dréau, M. Lesik, L. Rondin, P. Spinicelli, O. Arcizet, J.-F. Roch, and V. Jacques, “Avoiding power broadening in optically detected magnetic resonance of single NV defects for enhanced dc magnetic field sensitivity,” *Phys. Rev. B*, vol. 84, no. 19, p. 195204, 2011.
- [6.15] J. F. Barry, J. M. Schloss, E. Bauch, M. J. Turner, C. A. Hart, L. M. Pham, and R. L. Walsworth, “Sensitivity optimization for NV-diamond magnetometry,” *Rev. Mod. Phys.*, vol. 92, no. 1, p. 015004, 2020.